Kadir Kaan Karaveli AN ACCURATE INVESTIGATION OF THE MECHANICAL RESPONSE AND DAMAGE MODEL OF ALUMINUM 7068 AGU 2018

AN ACCURATE INVESTIGATION OF THE MECHANICAL RESPONSE AND DAMAGE MODEL OF ALUMINUM 7068

A THESIS
SUBMITTED TO THE DEPARTMENT OF ADVANCED MATERIALS AND NANOTECHNOLOGY
AND THE GRADUATE SCHOOL OF ENGINEERING AND SCIENCE OF ABDULLAH GUL UNIVERSITY
IN PARTIAL FULFILLMENT OF THE REQUIREMENTS
FOR THE DEGREE OF
MASTER OF SCIENCE

By
Kadir Kaan Karaveli
August 2018

AN ACCURATE INVESTIGATION OF THE MECHANICAL RESPONSE AND DAMAGE MODEL OF ALUMINUM 7068

A THESIS
SUBMITTED TO THE DEPARTMENT OF ADVANCED MATERIALS AND NANOTECHNOLOGYAND THE GRADUATE SCHOOL OF ENGINEERING AND SCIENCE OF ABDULLAH GUL UNIVERSITY
IN PARTIAL FULFILLMENT OF THE REQUIREMENTS
FOR THE DEGREE OF
MASTER OF SCIENCE

By
Kadir Kaan Karaveli
August 2018

SCIENTIFIC ETHICS COMPLIANCE

I hereby declare that all information in this document has been obtained in accordance with academic rules and ethical conduct. I also declare that, as required by these rules and conduct, I have fully cited and referenced all materials and results that are not original to this work.

Name-Surname: Kadir Kaan Karaveli

Signature :

REGULATORY COMPLIANCE

M.Sc.thesis titled AN ACCURATE INVESTIGATION OF THE MECHANICAL RESPONSE AND DAMAGE MODEL OF ALUMINUM 7068 has been prepared in accordance with the Thesis Writing Guidelines of the Abdullah Gül University, Graduate School of Engineering & Science.

Prepared By

Kadir Kaan Karaveli

Advisor

Assist. Prof. Burak Bal

Head of the Advanced Materials and Nanotechnology Program

Prof. Murat Durandurdu

Signature

ACCEPTANCE AND APPROVAL

M.Sc.thesis titled AN ACCURATE INVESTIGATION OF THE MECHANICAL RESPONSE AND DAMAGE MODEL OF ALUMINUM 7068and prepared by Kadir Kaan Karaveli has been accepted by the jury in the Advanced Materials and Nanotechnology Graduate Program at Abdullah Gül University, Graduate School of Engineering & Science.

…….. /…….. / ……..

(Thesis Defense Exam Date)

JURY:

Advisor : Assist. Prof. Burak Bal

Member : Assist. Prof. Benay Uzer

Member : Assoc. Prof. Emre Acar

APPROVAL:

The acceptance of this M.Sc.thesis has been approvedby the decision of the Abdullah Gül University, Graduate School of Engineering & Science, Executive Board dated ….. /….. / …….. and numbered ……..……. .

…….. /…….. / ……..

(Date)

Graduate School Dean

Prof. Dr. İrfan Alan

ABSTRACT

AN ACCURATE INVESTIGATION OF THE MECHANICAL RESPONSE AND DAMAGE MODEL OF ALUMINUM 7068

Kadir Kaan Karaveli

MSc. in Advanced Materials and Nanotechnology

Supervisor: Assist. Prof. Burak Bal

August 2018

The promising combination of high strength, high toughness, low density and corrosion resistivity have made aluminium (Al) alloys the material of choice in various applications, from buildings to aerospace, for decades. Especially, Al 7068 alloy is one of the recently developed materials used mostly in defence and automobile industries due to their exceptional mechanical properties. In this master thesis, the mechanical response and Johnson-Cook damage model of Al 7068-T651 alloy was investigated. Specifically, different Johnson-Cook damage parameters were determined for different application areas considering the maximum, minimum and average results. These damage parameters can be used for accurate Finite Element Analysis simulations. To determine these damage parameters tensile tests were conducted on notched and smooth specimen son both rolling direction and perpendicular to the rolling direction. The notch radius were selected as smooth, 0.4 mm, 0.8 mm and 2 mm to provide different stress triaxiality values and observe the mechanical response at these triaxiality values. Tensile tests were repeated seven times to obtain the accurate results. The final cross-sectional areas of fractured specimens were calculated through optical microscopy. The effects of stress triaxiality factor and rolling direction on the mechanical properties of Al 7068-T651 alloy were successfully investigated. All damage parameters were calculated via Levenberg-Marquardt optimization method.

Overall, three different Johnson-Cook damage parameters based on minimum, average and maximum equivalent strain values were calculated. These Johnson-Cook

damage parameters can be utilized for the accurate damage simulations of different applications in Finite Element Analysis, which is a computational technique and is used to obtain approximate solution of several engineering problems.

Keywords: Aluminum, Finite Element Analysis, Johnson-Cook damage model, Levenberg-Marquardt optimization method, tensile test, stress triaxiality.

ÖZET

ALUMİNYUM 7068 MALZEMESİNİN MEKANİK DAVRANIŞLARININ HASSAS OLARAK İNCELENMESİ VE HASAR MODELİNİN ARAŞTIRILMASI

Kadir Kaan Karaveli

İleri Malzeme ve Nanoteknoloji Bölümü Yüksek Lisans

Tez Yöneticisi: Dr. Öğr. Üyesi Burak Bal

Ağustos-2018

Yüksek mukavemet, yüksek tokluk, düşük yoğunluk ve korozyon dirençliliğinin ümit vaat eden kombinasyonu, onlarca yıldır alüminyum (Al) alaşımlarını binalardan havacılık sektörüne çeşitli uygulamalarda tercih edilen malzeme haline getirmiştir. Özellikle son zamanlarda geliştirilen malzemelerden bir tanesi olan Al 7068 alaşımı, olağanüstü mekanik ve mekanik özelliklerinden dolayı savunma sanayinde ve otomobil sanayinde kullanılmaktadır. Bu yüksek lisans tezinde, Al 7068-T651 alaşımının mekanik tepkisi ve Johnson-Cook hasar modeli araştırılmıştır. Özellikle, maksimum, minimum ve ortalama sonuçları dikkate alarak farklı uygulama alanları için farklı Johnson-Cook hasar parametreleri belirlenmiştir. Bu hasar parametreleri doğru Sonlu Elemanlar Analizi simülasyonları için kullanılabilir. Hasar parametrelerinin belirlenmesinde, hem hadde yönünde hem de hadde yönüne dik olarak çentikli ve düzgün numuneler üzerinde çekme deneyleri yapılmıştır. Çentik yarıçapı, farklı gerilim üçeksenliliği değerlerini sağlamak için pürüzsüz, 0,4 mm, 0,8 mm ve 2 mm olarak seçildi ve bu gerilim üçeksenliliği değerlerinde mekanik malzemenin tepkisi gözlemlendi. Çekme testleri, doğru sonuçları elde etmek için yedi kez tekrarlandı. Kırık numunelerin son kesit alanları optik mikroskop ile hesaplandı. Gerilim üçeksenliliği faktörünün ve hadde yönünün Al 7068-T651 alaşımının mekanik özellikleri üzerindeki etkileri başarılı bir şekilde araştırılmıştır. Tüm hasar parametreleri Levenberg-Marquardt optimizasyon yöntemi ile hesaplandı.

Sonuç olarak, minimum, ortalama ve maksimum eşdeğer gerinim değerlerine dayanan üç farklı Johnson-Cook hasar parametresi hesaplanmıştır. Bu Johnson-Cook

hasar parametreleri, bir hesaplama tekniği olan ve bu çeşitli mühendislik problemlerinin yaklaşık çözümünü elde etmek için kullanılan sonlu elemanlar analizinde farklı uygulamaların doğru hasar simülasyonları için kullanılabilir.

Anahtar Kelimeler: Alüminyum, Sonlu Element Analizi, Johnson-Cook hasar modeli, Levenberg-Marquardt optimizasyon metodu, çekme testi, gerilim üçeksenliliği.

Acknowledgements

I would like to express my great appreciation to my supervisor Assistant Professor Burak BAL for his extraordinary support, amazing patience and guidance throughout my thesis study. Moreover, I would like to thank İbrahim Burkay Tuğluca for his help during testing period.

In addition, I would also thank Berkay Gümüş and Aselsan A.Ş. for their support.

Also, I would like to express my sincere thanks to Turkuaz Seramik A.Ş. and its R&D Department; Kürşad Noyan Özkaya and Dinçer Yarımçam for their support.

Finally, I would also like to thank my family with my all heart; especially my wife Gökçe Yıldızhan Karaveli, my parents Engin and Nurten Karaveli, my step parents Necmi and Meltem Yıldızhan, my uncle Abdullah Buğrahan Karaveli and my friends; Ahmet Taha Karakaya, Muhammed Malik Tutal and Abdülvehab Yaman for their endless support, patience and love in my life.

Table of Contents

List of Figures

List of Tables

To My Family

Chapter 1

1 Introduction

The aim of this chapter is to summarize the aluminum's and its alloys' properties and application areas and the important previous works, including mechanical behavior under different conditions, Johnson-Cook (J-C) Material and Damage Models, which are used in Finite Element Analysis (FEA) to observe the material's mechanical response in the real usage areas, on aluminum alloys. The flowchart of this chapter starts with aluminum's and its alloys' production methods, general properties and classification methods, respectively. In the second part of this chapter, some specific literature on aluminum, J-C material & damage models and FE studies on aluminum and its alloys will be introduced.

1.1Aluminum and Its Alloy

Aluminum and its alloys are one of the most versatile, economical, and attractive metallic materials to be used a broad range of applications from both low density and high ductility required application areas to the most demanding engineering applications, such as aerospace industry, transportation, building, architecture and ordnance [1–4]. The main reasons why an aluminum and its alloys are one of the most attractive materials for several applications are their density values are relatively low, around 2.7 g/cm^3, and they show good corrosion resistance compared to other commercially used materials [2, 5]. Specifically, they are approximately one-third lighter than several steels and at the same time, some aluminum alloys are stronger than some steels [2, 6, 7]. Such combination of low density coupled with the high strength of several aluminum alloys makes them alternative material of choice in several application areas over most of the commercially

used steels [3]. In addition, due to the fact that they show significant ductility, their processing is not difficult.

1.1.1 Production of Aluminum from Bauxite to Raw

By mass, after oxygen and silicon, aluminum is the third most abundant element and the most abundant metal in the earth crust, approximately 8 percent [8]. The chemical affinity of aluminum is very high so it can be found as a compound with over 270 different minerals [9]. That's why it is hard to discover of aluminum. By using electricity to break down the chemical compounds in the element, the first aluminum was produced in 1824 and its industrial production was started in 1829 [10].

The production of aluminum obtain two steps, which are refining bauxite to alumina and electrolyzing alumina to melted aluminum, respectively [8]. Firstly, bauxite is a clay mineral that contains mostly various types of aluminum hydroxide mixed with other elements [8]. Bauxite is processed into alumina (Al_2O_3). In the second step, by using electrolytic reduction cells, it is processed into aluminum. Then casting process of aluminium is carried out with adding very small amount of admixtures that can effect on the properties so it opens new application areas to aluminum [11]. This process, which is called as Bayer Process, was invited by Karl Bayer in 1887 and patented in 1888 [9, 10].

1.1.2 Classification of Aluminum Alloys

According to different primary mechanisms of property development, there are two main types of aluminum alloys: wrought compositions and cast compositions [2, 12]. In this chapter, wrought aluminum alloys will be investigated. There are several types of wrought aluminum alloys based on alloying elements [13–15]. The effects of alloying elements on several material properties and application areas of alloys are given in Table 1.1.2.1 [4, 13, 16, 17].

Alloy Designation [14]	**Alloying Element**	**Properties**	**Application Areas**
1xxx	%99 Pure Aluminum Iron and Silicon are major impurities.	➢ Excellent corrosion resistance, ➢ High thermal and electrical conductivity, ➢ Low mechanical properties, ➢ Excellent workability	Electrical and chemical fields
2xxx	Copper	➢ Poor corrosion Resistance, ➢ Heat treatment condition mechanical properties are high (similar to mild steel)	Aircraft where their high strength demand (most widely used aircraft alloy)
3xxx	Manganese	➢ Non-heat treatable, ➢ Good workability	Architectural applications and its various products

4xxx	Silicon	➢ Low melting point ➢ Non-heat treatable	Welding rods, Brazing sheets, Architectural applications
5xxx	Magnesium	➢ Most widely used aluminum alloy, ➢ Moderate to high strength, ➢ Non-heat treatable, ➢ Good welding characteristic, ➢ Good corrosion resistance in marine atmosphere,	Boat hulls, Gangplanks, Other products exposed to marine environments
6xxx	Magnesium and Silicon (Magnesium Silicate)	➢ Heat-treatable, ➢ Good formability, ➢ Good corrosion resistance, ➢ Medium strength,	Architectural extrusions, Automotive components
7xxx	Zinc	➢ Heat-treatable alloys of very high strength when combined with small percentage of magnesium, ➢ Highest strength alloys	Air–frame structures, For highly stressed parts

8xxx	Tin, Lithium, and/or Iron.	Higher strength, better formability, and improved stiffness than 1xxx series aluminum alloys.	Suitable for thinner gauge applications.

Table 1.1.2.1Aluminum alloy series, their properties and application areas

1.1.3 Heat Treatment of Aluminum Alloys

Aluminum alloys can be also classified as heat-treatable or non-heat-treatable, whose mechanical properties are achieved by cold working, such as rolling and extrusion [18]. For heat-treatable alloys, the strength can be enhanced by addition of alloying elements. They can also increase the solid solubility in aluminum with increasing temperature. The most important alloying elements in heat-treatable alloys are copper, lithium, magnesium, and zinc [12]. The heat-treatment cycle is started with solution treatment that is occurred at high temperature to maximize the solubility. Then rapid cooling or quenching step is applied to reach low temperature quickly. In this step, solute atoms, which are clustered together, form precipitates that are coherent with the matrix. Thus, a supersaturated solid solution with both solute elements and vacancies is obtained. After quenching alloys is not stable at room or elevated temperatures and precipitations of constituents from supersaturated solution begins. This process is called as aging.

In general, there are two different aging processes. These are, natural ageing (T1, T2, T3, and T4) and artificial ageing (T5, T6, and T9). The difference between these ageing processes are natural ageing process occurs spontaneously at ordinary temperature until the metal reaches a stable condition, but artificial ageing process is controlled and it does not happen spontaneously. Thus, the increase in strength after solution heat-treating in artificial ageing is quicker and higher than natural aging [13, 18].

1.1.4 7000 Series Aluminum Alloys

Due to zinc, that is the major alloying element of 7000 series aluminum alloys, and small amount of magnesium, which makes them heat-treatable, these alloys are known as the strongest aluminum alloys [5, 19]. Their density values make them a suitable material when weight to strength ratio is critical for demanding application. However, its corrosion resistance is poor. Actually, it is lower than other aluminum alloys [20]. Their application areas are mostly aerospace, ordinance, building, transportation and military [21].

1.1.4.1 Al 7068 T651 Alloys

Al 7068 alloy was designed to meet the needs of applications, where the combination of high strength and low density is required. This alloy is the strongest aluminum alloy among all Al series [22]. Yield strength values of this alloy can reach up to 700 MPa, its ductility is minimum 5%, which may be reach up to 40%, with good corrosion resistance, and other features make this alloy more suitable for high performance demanding applications [23]. Therefore, 7068 is capable of increasing the strength or reduce the weight/cross section ratio of the critical components. In addition, different temper systems have different effects on the mechanical properties of this alloy. For instance, T651 explains heat treatment process, which is solution heat-treated and stress relieved by stretching then artificially aged.

Typical Physical Properties of Al 7068 [20]	
Density at 20°C	2.85 kg/dm^3
Melting Range	476 - 635°C
Specific Thermal Capacity at 100°C	1050 $J.Kg^{-1}.K^{-1}$
Mean Coefficient of Thermal Expansion	23.4 $10^{-6}.K^{-1}$

(20 - 100°C)	
Thermal Conductivity at 20°C	190 $W.m^{-1}.K^{-1}$
Electrical Conductivity at 20°C T6511	31 % IACS
Electrical Conductivity at 20°C T76511	39 % IACS
Young's Modulus	73.1 GPa

Table 1.1.4.1.1 Some of physical properties of Al 7068

Minimum Mechanical Properties of Al 7068 (Extruded Bar) [20]		
Temper	**UTS (MPa)**	**Elongation (%)**
T6 / T6511	683	5
T6 / T6511	648	5
T76 / T76511	593	7

Table 1.1.4.1.2 The effect of different temper systems on the mechanical properties of Al 7068

Chapter 2

2 FINITE ELEMENT ANALYSIS

The finite element analysis (FEA) is a computational technique for solving engineering problems [24]. A typical work principle for this method is divided into two steps. First step is dividing a complex problem into small elements, followed by recombining all sets of element equations into a global system of equations for final calculations [25, 26].

Though the mathematical roots of FEA have been using for a long time, the FEA was really started in the 1940s by introducing the concept of piecewise-continuous functions in a sub-domain [24]. Nowadays, it is used to solve several engineering problems, such as mass transport, electromagnetic potential, fluid flow, and structural analysis. By using this method, the number of physical prototypes and experiments trials can be reduced.

One of the most important parameters to run FEA is material model. Different material models can give different results and each material model is capable of different things. For instance, one material model can capture both strain rate hardening and thermal softening, while one can capture only one of them. In the literature, there are several material models for Finite Element Analysis and some of them are listed in Table 2.1.

Material Model	**Expression**

Poulachon's Model and Poulachon-IEP's Model [27]	$\sigma = (A + B\varepsilon^{-n})(1 - CT)$
Huang's Model [28]	$\sigma = (A + B\varepsilon^{n})(1 - C\ln\dot{\varepsilon})\left\|1 - \left(\frac{T_{melt} - T}{T_{melt} - T_{room}}\right)^{m}\right\|$
Johnson Cook's Model [29]	$\sigma = [A + B\varepsilon^{n}][1 + CLn(\dot{\varepsilon^{*}})][1 - T^{*m}]$
Zerilli-Armstrong Model [30]	$\sigma = A + \left[\, C_1 + C_2\sqrt{\varepsilon}\right]e^{\{-C_3 + C_4\ln(\dot{\varepsilon})\}T} + C_5\,\varepsilon^{n}$
Koppka's Model [31]	$\sigma = [B\varepsilon^{n}]\left[1 - Cln\left(\frac{\dot{\varepsilon}}{1000}\right)\right]\left[\left(\frac{T_{melt} - T}{T_{melt} - T_{room}}\right)^{m} + ae^{-0.00005(T-700)^{2}}\right]$
Umbrella's Model [32]	$\sigma = B(T)(C\varepsilon^{n} + F + G\varepsilon)[1 + (\ln(\dot{\varepsilon})^{m} - A)]$
El-Magd's Model [31]	$\sigma(\varepsilon, \dot{\varepsilon}, T) = (K(B + \varepsilon)^{n} + \eta\dot{\varepsilon})exp\left[-\beta_1\frac{T - T_0}{T_m}\right]$

Sheppard-Wright's Model [33]	$\bar{\sigma} = \frac{1}{\alpha}\ln\left\{\left(\frac{Z}{A}\right)^{\frac{1}{n}} + \left[1 + \left(\frac{Z}{A}\right)^{\frac{2}{n}}\right]^{\frac{1}{2}}\right\}$

Table 2.1 Material Models using in FEA

where σ is the flow stress (von Mises stress), ε is the plastic strain, A is the yield stress at reference temperature and reference strain rate, B is the coefficient of strain hardening, n is the strain hardening exponent,a range of testing conditions, C and m are the material constants which represent the coefficient of strain rate hardening and thermal softening exponent, respectively. Z is temperature compensated strain rate parameter or Zener-Hollomon parameter. F and G are functions of steel hardness (HRC). K is strength coefficient of material.β_1 and η material constants.$\dot{\varepsilon^*} = \dot{\varepsilon}/\dot{\varepsilon}_0$ is the dimensionless strain rate with $\dot{\varepsilon}$ the strain rate and $\dot{\varepsilon}_0$ the reference strain rate, and T* is the homologous temperature and expressed as $T^* = \left(T - T_{ref}\right)/\left(T_m - T_{ref}\right)$. Here, T is the absolute temperature, T_m the melting temperature and $T_{ref}$the reference temperature.

Chapter 3

3 PREVIOUS STUDIES

The aim of this chapter is to review the recent studies on the Johnson-Cook damage model and Finite Element Analysis of aluminum and its alloys for several applications. Significant studies related to the present study are summarized below.

3.1 Previous Studies on Johnson-Cook Damage Model of Aluminum and Its Alloys

3.1.1 Gordon R. Johnson and William H. Cook [1985]

There is a tendency to distinguish the dynamic material properties from the static material properties. The reason of the difference between these properties is the strain rate effect. In this paper [34], fracture characteristics of copper, iron and 4340 steel were investigated by torsion test over a range of strain rates. In addition, Split-Hopkinson bar tests at high temperatures, and quasi-static tensile tests were conducted. The results were used in cumulative damage fracture models, which express the equivalent plastic strain for damage initiation as a function of strain rate, temperature and stress. This model is called as Johnson-Cook damage model. [34].

3.1.2 A. Manes, L. Peroni, M. Scapin and M. Giglio [2011]

In this study [35], the strain rate effect on the mechanical behavior of Al 6061 T6 alloy was investigated by several dynamic testing methods to generate a data under dynamic conditions. Bilinear function was used to approximate the strain rate dependence and Johnson Cook material model, which is one of the most widely used material models, in numerical simulations. In order to obtain J-C material model parameters a numerical optimization was used. Thus, in this work, material model identification was carried out by focusing on the strain rate sensitivity identification since Al 6061 T6 alloy can be subjected to the ballistic impact loadings [35].

3.1.3 Nachhatter S. Brar and Vasant S. Joshi [2012]

In this study [36], different constitutive material models of high strength 7075-T651 aluminum alloy were discussed. The samples were subjected to tension, compression and torsion loadings at low and high strain rates and different temperatures. The mechanical response results were used as an input for the determination of Johnson-Cook material model constants of Al 7075-T651 plates and bars. The calculated parameters can be used for impact simulations. As a result of their work, they observed that this alloy shows anisotropic material properties at high strain rate [36].

3.1.4 Ding-Ni Zang, Qian-Qian Shangguan, Can-Jun Xie and Fu Liu [2014]

In this study [4], the effect of strain rate on the mechanical properties of Al 7075-T6 alloy was observed by conducting uniaxial quasi-static and dynamic tensile tests. Modified Johnson-Cook models, which include some modifications like the strain hardening, strain rate hardening or the temperature softening terms to improve the accuracy of original J-C model, described the relationship between the flow stress and strain rate. In addition, the parameter C in the strain rate hardening term of J-C

constitutive equation was modified as a function of strain rate. Thus, a modified J-C model was constructed by using the experimental results [4].

3.1.5 Jin Qiang Tan, Mei Zhan, Shuai Liu, Tao Huang, Jing Guo and He Yang [2014]

In this study [37], by using a modified Johnson-Cook model, the tensile flow behaviors of 7075-T7451 aluminum alloys at high strain rates were described. The samples were subjected to the uniaxial quasi-static and dynamic tensile tests at different strain rates (10^{-3} s^{-1}, 800 s^{-1}, 1900 s^{-1} and 2900 s^{-1}). As a result of this study, it was shown that modified J-C model gives higher prediction accuracy to describe tensile flow behavior for Al 70750-T7451 alloy at high strain rates than original J-C model and Khan-Liu (K-L) model [37].

3.1.6 Yancheng Zhang, J.C. Outerio and Tarek Mabrouki [2015]

In this study [29], an analysis of two sets of Johnson-Cook model parameters for Ti-6Al-4V was performed for three types of metal cutting models that are Lagrangian (LAG), Arbitrary Eulerian-Lagrangian (ALE) and Couple Lagranian-Eulerian (CEL). The aim of this study is to find an answer of the most suitable Johnson-Cook model parameters for a given material. Consequently, test results showed that Johnson-Cook model parameters are not unique for the three numerical models of metal cutting [29].

3.1.7 Ravindranadh Bobbili, Ashish Paman and V. Madhu [2016]

The aim of this study [38] is to obtain Johnson-Cook constitutive models constants forAl-4.8Cu-1.2Mg alloy. To obtain these constants tensile tests were conducted at different stress triaxiality values, at different strain rates ranging from 0.1 to 3500 s^{-1}andat different temperatures (25, 100, 200 and 300 ℃). After tensile tests, SEM images of fracture surface were taken to observe the void formations on this alloy and micro-voids and dimples indicate the ductile fracture mode. Overall results show that modified J-C model is suitable for this alloy to predict flow tensile flow behaviors at high strain rates

and temperatures, and modelling results matched very well with experimental results [38].

3.2 Previous Studies on Finite Element Analysis

While it is difficult to determine the date of invention of Finite Element Analysis (FEA), it originated from the need to solve complex engineering problems, such as elasticity and structural analysis. In this part, studies on FEA material models have been investigated chronologically.

3.2.1 R. Courant [1943]

In this study [39] the new variational form, which was an independent rediscovery of a simpler method, was presented briefly. This method mainly deals with boundary value and eigenvalue problems. In addition, the first efforts to use piecewise continuous functions over triangular domains were defined into the applied mathematics literature. R. Courant's approach, developed in early 1940s, divides the domain into smaller finite triangular sub-regions and solves second order elliptic partial differential equations (PDEs). This pioneer study has significant effects on the development of Finite Element Method [39].

3.2.2 O.C. Zienkiewiez, R.L. Taylor and J.Z. Zhu [1967]

The finite element method obtained its real impact from O.C. Zeinkiewiez's and his co-workers' study. Their book [40] explained the distinction between finite element analysis and finite difference method. According to their explanation, the finite difference method is just a mathematical approximation while finite analysis is a physical one, based on integral scheme. To sum up, their work explained the basic of finite element approach, which is now used in many applications as a powerful and versatile technology [40].

3.2.3 Ernest Hinton and Bruce Irons [1968]

In this paper [41], Finite Element Method (FEM) was used to interpret the strain patterns. This paper explained the method of least squares, their problems and the solutions of these problems by FEM. Some of these problems were interpolation, re-entrant boundaries, local stress concentrations and introducing prescribed values at the boundaries. As a conclusion of this work, they compare the results of conventional and Finite Element methods and show that finite element method gives quicker results than conventional methods [41].

3.2.4 Gilbert Strang and George J. Fix [1973]

This book [42] explains the connection of the finite element method with the established Reyleigh-Ritz-Galerkin method, which is used to minimize the error function or residual, so that the approximation can reach close to the actual solution. In addition to elliptic problems, it affects eigenvalue and initial-value problems and problems with singularities. Overall, this book explains the effects of each approximation methods that are important for the finite element analysis to make it computationally efficient. This approximation is staring from a given physical problem and it includes interpolation of the original physical data, choice of a finite number of polynomial trial functions, simplification of the geometry of the domain, modification of the boundary conditions, numerical integration of the underlying functional in the variational principle and rounding error in the solution of the discrete system [42].

Chapter 4

4 Determination of Johnson-Cook Damage Model Parameters and Mechanical Properties of Aluminum 7068 Alloy

4.1 Abstract

Al 7068-T651 alloy is one of the recently developed materials used mostly in the defence industry due to its high strength, toughness and low weight compared to other steels. The aim of this study is to identify the accurate Johnson-Cook (J-C) damage parameters of the Al 7068-T651 alloy for Finite Elemental Analysis (FEA) based simulation techniques. In order to determine these parameters, tensile tests were conducted on notched and smooth specimens at medium strain rate, 1/s. Tests were repeated 7 times to ensure the consistency of the results both in the rolling direction and perpendicular to the rolling direction. The final areas of fractured specimens were calculated through optical microscopy. The effects of stress triaxiality factor and rolling direction on the mechanical properties of Al 7068-T651 alloy were investigated. All damage parameters were calculated via Levenberg-Marquardt optimization method. In this article, J-C damage model constants, based on maximum and minimum equivalent strain values, were also reported which can be utilized for the simulation of different applications.

4.2 Introduction

High strength and lightweight materials have become the materials of choice for several applications [3]. Among other metallic materials, aluminum (Al) alloys, which have face-centred cubic (FCC) crystal structure at room temperature, are one of the most popular materials due to their promising mechanical properties [2, 17]. Aluminum 7000 series has been widely used in automobile, machinery, aerospace and defence industries due to its excellent combinations of low weight, high strength, good machinability and high corrosion resistance [5, 15]. Al 7068-T651 alloy is the strongest aluminum commercially produced with 6-8% zinc as a predominant element in its chemical composition [20]. In the mid 1990's, this alloy was developed by Kaiser Aluminum and designed as an alternative to Al 7075 alloys for applications which require greater strength at both room and elevated temperatures. In particular, compared to Al 7075 alloy, it has similar corrosion resistance, promising ductility and 30% higher yield strength [20, 21]. Thus, Al 7068-T651 alloy, which has greater strength and lower weight than Al 7075, is a better material of choice for several industries, such as automotive, aviation and defence. Therefore, the precise determination of the mechanical response of Al 7068 alloy and the development of a constitutive material and damage model are of paramount importance to increase the accuracy of finite element analyses (FEA) and to utilize this material on the aforementioned applications.

Different plasticity and failure models have been developed to describe the flow stress and deformation behavior of materials under various conditions in finite element modelling (FEM) for different applications (Figure 4.2.1). Among others, Johnson-Cook (J-C), which includes strain hardening, strain rate hardening and thermal softening, is the most widely used material model [43]. Therefore, the precise determination of J-C damage parameters is of most importance to obtain the realistic FEM results. J-C damage parameters are generally obtained by the material response under tensile or Split-Hopkinson loading scenarios [44]. Due to the nature of materials, several factors affect this material response, such as rolling direction, temperature and strain rate. In the current literature, the effects of temperature and strain rate have been well studied but the effect of rolling direction on J-C damage parameters have not been investigated in detail [45].

First, the number of experimental repetitions used in these studies to ensure the consistency of material response is not enough to determine precise J-C damage parameters. Second, the J-C damage parameters are determined by considering only the average equivalent failure strain. Consequently, to the best of the authors' knowledge, there is no study, which determines the Johnson-Cook damage model parameters of Al 7068-T651 considering different rolling directions, with a high number of experimental repetitions, and aiming different applications.

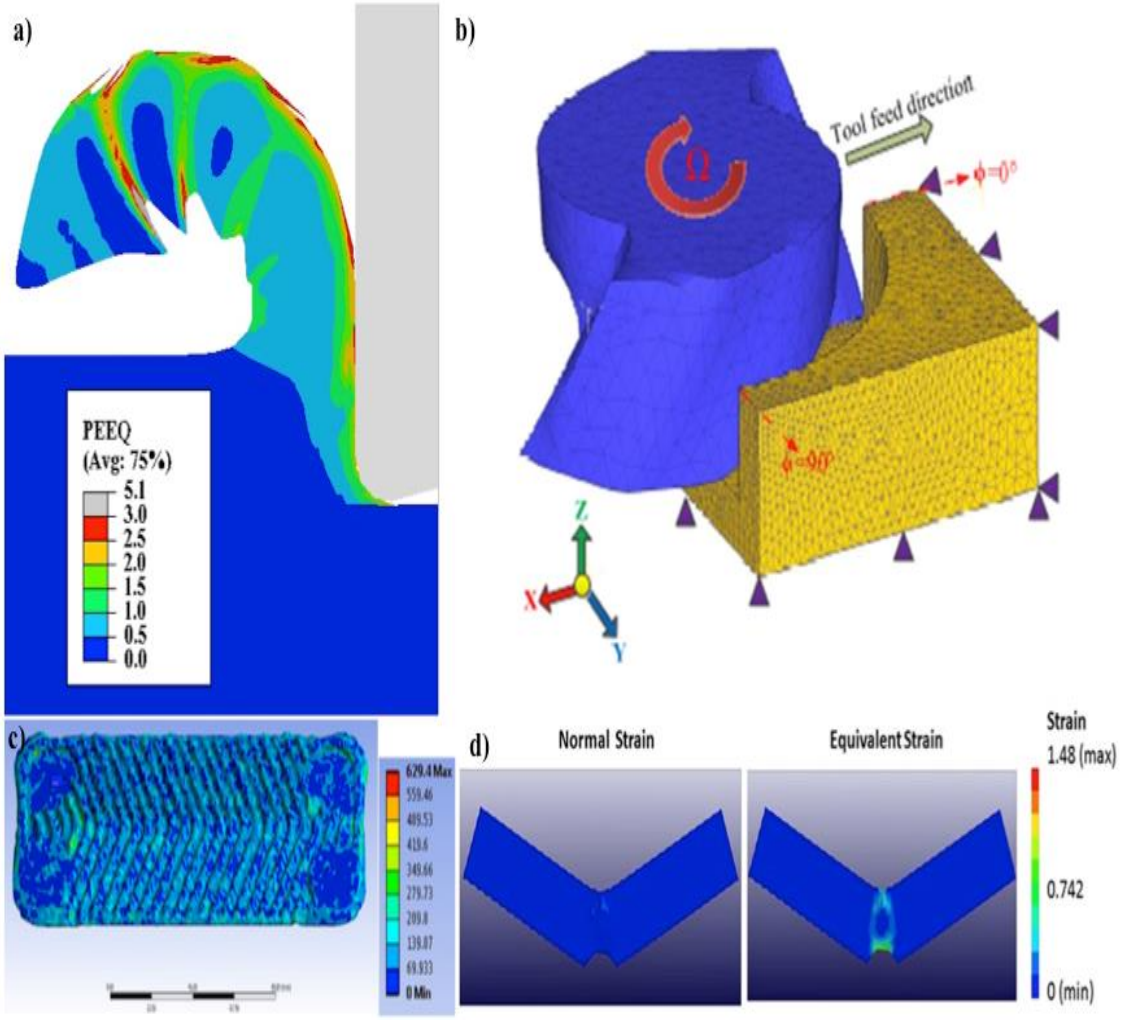

Figure 4.2.1 Examples of Finite Elemental Analysis a) the distribution of the equivalent plastic strain (PEEQ), of Ti-6Al-4V [29]**, b) 3-D FE model for half-immersion micro-end milling** [46]**, c) Heterogeneous equivalent stress distribution on steel plate simulation** [47]**, d) Demonstration of differences in normal and equivalent and strain fields upon a typical impact simulation of niobium-zirconium alloy** [48]

In this study, tensile tests at medium strain rate, i.e. 1/s, were conducted 7 times to ensure the consistency of results. Samples were taken from materials in both the rolling

direction and perpendicular to the rolling direction to determine the J-C damage parameters of Al 7068-T651 alloy precisely. Therefore, both the effects of rolling direction and stress concentration, induced by notch on the sample surface to produce localized plasticity, on the overall material response of the Al 7068-T651 alloy were determined. Moreover, using maximum, average and minimum equivalent failure strain values, different J-C damage parameters were determined for several applications. In order to solve an overdetermined system and to obtain J-C damage parameters for different application areas, an iterative Levenberg-Marquardt least squares method was used. In particular, the methodology of the Levenberg-Marquardt least squares method was transferred to the Matlab environment. Overall, the work presented herein exhibits the precise J-C damage parameters, which can be used for accurate damage simulations in FEA for different application areas of Al 7068-T651 alloy, as well as the effects of rolling direction and notch radius on the material response of Al 7068-T651 alloy.

4.3 Experimental Procedures and Results

Aluminum 7068-T651 alloy is the investigated material in the current study. The chemical composition of the studied material is illustrated in Table 4.3.1 In order to produce this material, solution heat treatment process was applied to Al 7068 alloy, which is then stress relieved by stretching and then artificially aged. By turning and milling operations, tensile test specimens were prepared and then polished to get rid of all flaws and residual stresses on the material's surface. The samples were prepared in two groups: along the rolling direction and perpendicular to the rolling direction.

Fe	Cu	Mn	Mg	Cr	Zn	Zr	Si
0.15	1.6	0.1	2.9	0.05	7.9	0.05	0.13

Table 4.3.1 Chemical composition of the studied material (in wt. %)

In order to determine the effects of stress triaxiality, corresponding mechanical behavior and J-C damage parameters, samples were subjected to tensile loading at room temperature. J-C damage parameters were calculated using stress and strain data of specimens whose technical drawings are shown in Figure 4.3.1, where R represents the

notch radius of the notched specimens. There were four different specimen types: smooth one and three notched specimens with different notch radii. Designing different specimens introduces different stress triaxiality factors (STF), σ^*, which are listed in Table 4.3.2.

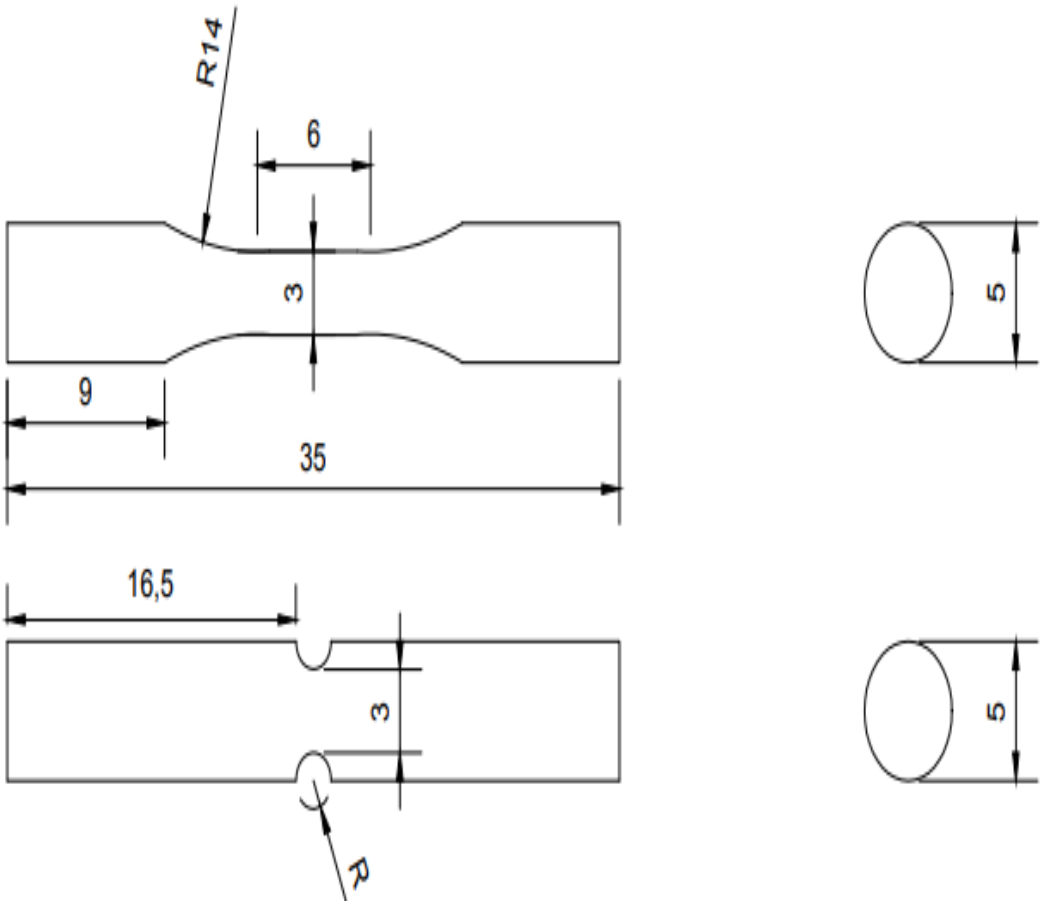

Figure 4.3.1 Specimen dimensions of smooth specimen and notched specimen for tensile testing (unit:mm)

A servo-hydraulic tensile/fatigue test machine, Instron 8801, was utilized to conduct tensile tests at a strain rate of 1/s and at room temperature. Since specimens have insufficient length to fit in the distance between the jaws of the test equipment, a couple of fixtures were used during tensile tests (Figure 4.3.2). The initial and final positions after fracture are shown in Figure 4.3.2(a) and Figure 4.3.2(b), respectively.

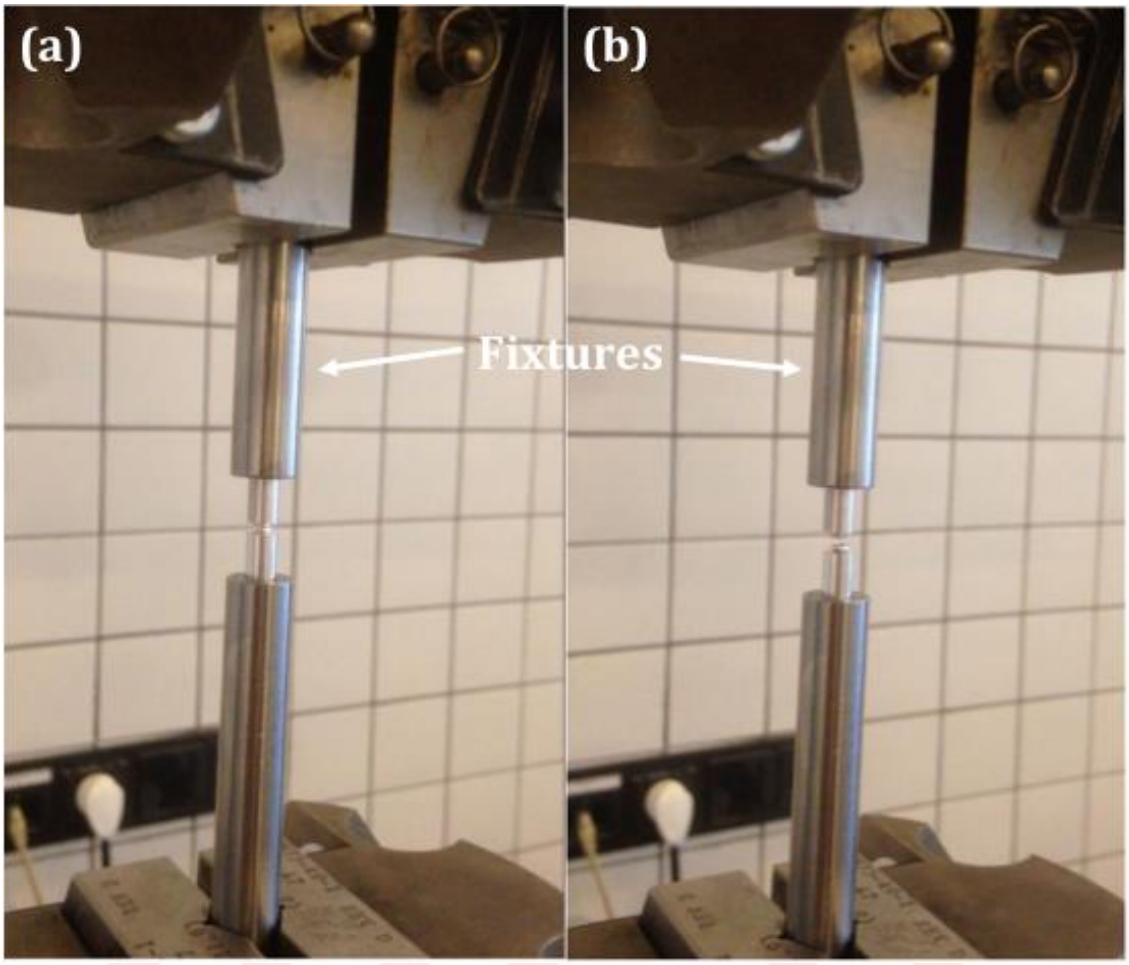

Figure 4.2.2 Experimental setup for material test by servohydraulic tensile/fatigue test machine at a strain rate of 1 x 100 s-1 and room temperature (a) initial position of the specimen (b) position after fracture

To ensure the accuracy of results, seven identical samples were tested. In total, 56 tensile tests were performed, consisting of eight sample types and seven repetitions. Displacement and force data were measured by the extensometer and load cell of the servo-hydraulic tensile/fatigue test machine, respectively. By using classical elasticity-plasticity equations, both engineering and true stress and strain values of specimens were obtained [49].

After the tensile tests, the diameters of the ellipsoidal fractured cross sectional areas of the specimens were measured by an optical microscope, EUROMEX NexiusZoom (Figure 4.3.3). The corresponding cross sectional areas were then calculated from the classical ellipse equation that is defined as:

$$x^2/a^2 + y^2/b^2 = 1 \qquad (4.3.1)$$

where x and y are the coordinates of a point on the ellipse, and a and b are the radii on the x and y coordinates, respectively.

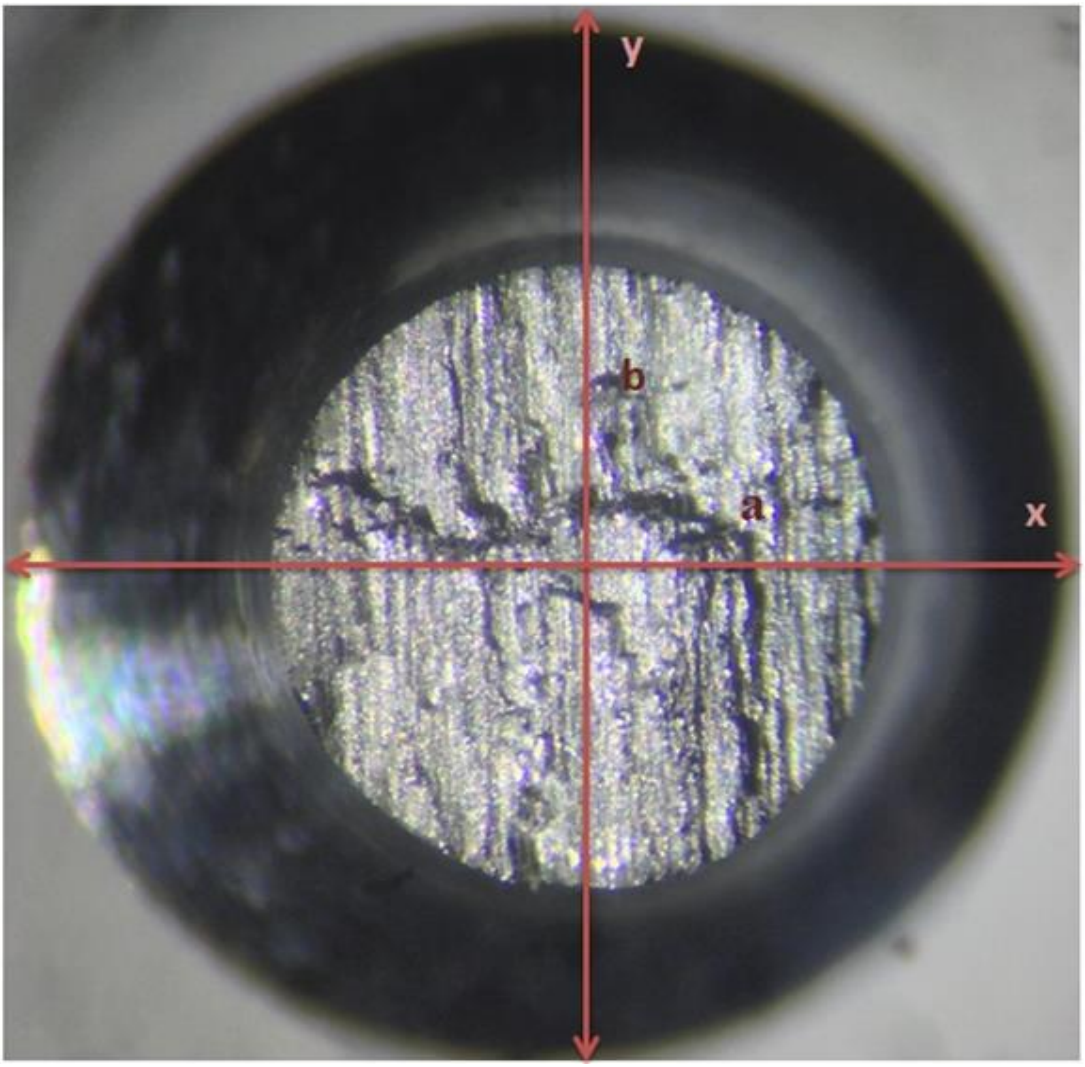

Figure 4.3.3 Calculation of the final cross-section area of the specimens.

4.4 Theory and Calculations

The empirical J-C model is practical for describing the stress and strain relations of metals under conditions of large deformation, high strain rate and high temperature [38]. By using limited data from experiments, J-C model well predicts the mechanical properties of metals. The general expression can be defined as:

$$\sigma = [A + B\varepsilon^n][1 + CLn(\dot{\varepsilon}^*)][1 - T^{*m}] \quad (4.4.1)$$

whereσ is the equivalent flow stress, A is the yield stress of the material under reference deformation conditions (unit is MPa), B is the strain hardening constant (unit is MPa), C is the strain rate strengthening coefficient, n is the strain hardening coefficient, m is the temperature softening of the material through homologous temperature, $T^*.\dot{\varepsilon}^*$ is the dimensionless strain rate $[\dot{\varepsilon}^* = \dot{\varepsilon}/\dot{\varepsilon}_0]$ where $\dot{\varepsilon}$ is the equivalent plastic strain, and $\dot{\varepsilon_0}$ is the reference strain rate. T^*can be calculated through $T^* = \left(T - T_{ref}\right)/\left(T_m - T_{ref}\right)$ where $T_m$is the melting temperature of the material and T_{ref} is the reference deformation temperature. In equation 4.4.1, $[A + B\varepsilon^n]$ and $[1 + CLn(\dot{\varepsilon}^*)]$ represent the effects of strain hardening and strain rate strengthening, respectively, while $[1 - T^{*m}]$ stands for the effect of temperature.

The J-C fracture criterion makes the failure strain sensitive to stress triaxiality, temperature, strain rate and strain path. This model interests in damage accumulation via damage parameter. D, in equation 4.4.2, is damage variable, [0, 1]. When D is equal to 0, the material is not damaged, when it is equal to 1, the material is fully damaged. D can be defined as:

$$D = \sum_{t=0} \left(\Delta\varepsilon_{pl}/\dot{\varepsilon}\right) \quad (4.4.2)$$

where $\Delta\varepsilon_{pl}$ is the variation of the equivalent plastic strain.

According to the J-C ductile failure model, the equivalent plastic strain for damage initiation, $\bar{\varepsilon_f}^{pl}$, depends on stress triaxiality, strain rate and temperature and it can be defined as:

$$\bar{\varepsilon}_f^{pl}(\sigma^*, \dot{\bar{\varepsilon}}^{pl}, T^*) = \left[D_1 + D_2 e^{D_3\sigma^*}\right][1 + D_4 Ln(\dot{\varepsilon}/\dot{\varepsilon_0})][1 + D_5 T^*] \quad (4.4.3)$$

where D_1, D_2, D_3, D_4 and D_5 are J-C damage parameters. These parameters can be calculated from the tensile test results. The expression in the first set of brackets represents the effect of STF. The second and the third brackets represent, respectively, strain rate effect and temperature effect. In this study, constants D_1, D_2 and D_3 were determined by performing tensile test at medium strain rate, 1/s, on notched specimens (notch radii, 0.4 mm, 0.8 mm, and 2.0 mm) and smooth specimens at room temperature. Stress Triaxiality Factor (STF) is the ratio of hydrostatic stress to equivalent stress and is found in the range [−∞, +∞]. It can be expressed as:

$$STF = [\sigma_h/\sigma] \tag{4.4.4}$$

where σ_h is hydrostatic stress and σ is equivalent stress, which proves that the J-C failure model depends on the STF. On the other hand, a newer factor is used in the failure analysis of ductile metals, which is called the Lode angle or the Lode parameterθ_L. This parameter or angle is the third invariant of deviatoric stress tensor [50].

The characteristic values of STF are 1/3 for uniaxial tensile stress (σ, 0, 0) with σ>0, and -1/3 under uniaxial compression (σ, 0, 0) with σ<0 for a smooth material [51]. Since notched specimens have more local deformation, STF changes and can be expressed as:

$$\sigma^* = (1/3) + Ln(1 + a_0/2R_0) \tag{4.4.5}$$

where a_0 is the specimen radius at the notch center and $R_0$is the original specimen radius. STF values for each specimen are listed in Table 4.4.1.

Notch Radius (mm)	**Gauge Length (mm)**	$\boldsymbol{\sigma^2}$
Smooth	5	0.33

R0.4	0.74	1.39
R0.8	1.52	0.99
R2	3.46	0.65

Table 4.4.1 Stress triaxiality factors and gauge lengths for each configuration

In order to determine J-C failure model constants, the equivalent plastic strain at failure, $\bar{\varepsilon}_f^{pl}$ is calculated by the Equation 44.6, where A_0 and A_f are the initial and final cross-section areas, respectively. After tensile test, the final cross sections of specimens are assumed to be elliptic and their diameters, which are perpendicular to each other, are measured with an optical microscope. Final cross-section areas of the specimens were calculated from the classical area of an ellipse equation. The calculated initial and final cross-section areas of the specimens are given in Table 4.4.2.

$$\bar{\varepsilon}_f^{pl} = Ln\, A_0/A_f \tag{4.4.6}$$

Rolling Direction	**Notch Radius (mm)**	**Initial Area (mm^2)**	**Final area (mm^2)**
Along The Rolling Direction	Smooth	7.06	5.78
	0.4	7.06	6.44
	0.8	7.06	6.07

	2	7.06	6.00
Perpendicular To The Rolling Direction	Smooth	7.06	6.81
	0.4	7.06	6.97
	0.8	7.06	7.02
	2	7.06	6.60

Table 4.4.2 Initial and fracture cross-section areas of the specimens

To calculate Johnson-Cook damage parameters, D_1, D_2 and D_3, strain rate and temperature are assumed as stationary, therefore equation 4 can be expressed as:

$$\bar{\varepsilon}_f^{pl}(\sigma^*, \dot{\bar{\varepsilon}}^{pl}, T^*) = \left[D_1 + D_2 e^{D_3 \sigma^*}\right] \tag{4.4.7}$$

In this study, there are 4 specimens, one of them is smooth and others are notched, which results in 4 equations for both materials in the rolling direction and perpendicular to the rolling direction. In equation 4.4.7, there are 3 unknowns,D_1, D_2 and D_3. Therefore, to solve the overdetermined system the Levenberg-Marquardt optimization method was utilized and J-C damage parameters were calculated. The optimization code was prepared in Matlab.

4.5 Results and Discussion

The mechanical responses of notched and smooth Al 7068 alloys along the rolling direction and perpendicular to the rolling direction at room temperature and at medium strain rate, 1/s, are illustrated in Figure 4.5.1, and the corresponding mechanical properties are listed in Table 4.5.1. The force displacement and true stress-true strain graphs of both along and perpendicular to rolling direction specimens are given in Figure 4.5.1(a-d). It

is clear that the mechanical properties of the Al 7068 alloy depend on both the rolling direction and notch radius, which alters STF. Specifically, the specimen along the rolling direction with a 0.4 mm notch radius, which has the highest STF, shows the best, and the smooth specimen shows the worst ductility and strength combination. On the contrary, the smooth specimen has higher strength values at the same strain values in the elastic range compared to other specimens, even though it shows less ductility than others. Also, smooth specimen shows more plasticity than notched specimens (Figure 4.5.1(c)). This result can be attributed to the fact that notched specimens spend the given energy to the localized deformation around the notched region elastically but cannot accommodate the given energy plastically. On the contrary, the deformation is uniform for the smooth specimens and the energy can be accommodated plastically for a certain period of time prior to the failure. Furthermore, as the STF increases, both ductility and strength values of Al 7068 alloy along the rolling direction also increase. The ductility of the material increased from 0.1 to 0.5 and strength of the material increased from 819 to 1510 MPa with increasing STF. When compared to the Al 7075 alloy, these results show that Al 7068 alloy along the rolling direction shows a better strength and ductility combination [36].

Figure 4.5.1(b) and Figure 4.5.1(d) show the force-displacement curves and true stress-true strain curves of Al 7068-T651 alloy perpendicular to the rolling direction at room temperature and a strain rate of 1/s, respectively. It can be observed that the specimen with a 0.8 mm notch radius has a higher strength value than other specimens. However, the specimen with a 0.4 mm notch radius has the best ductility. In contrast to the rolling direction case, the specimen with a 0.4 mm notch radius has the lowest strength value and the specimen with a 2 mm notch radius has the lowest ductility. Similar to the rolling direction case, as the STF increases, ductility of the specimens that are perpendicular to the rolling direction also increases from 0.05 to 0.19. When compared to the Al 7075 alloy along the rolling direction, these results show that Al 7068 alloy perpendicular to the rolling direction shows weaker mechanical strength and ductility [52].

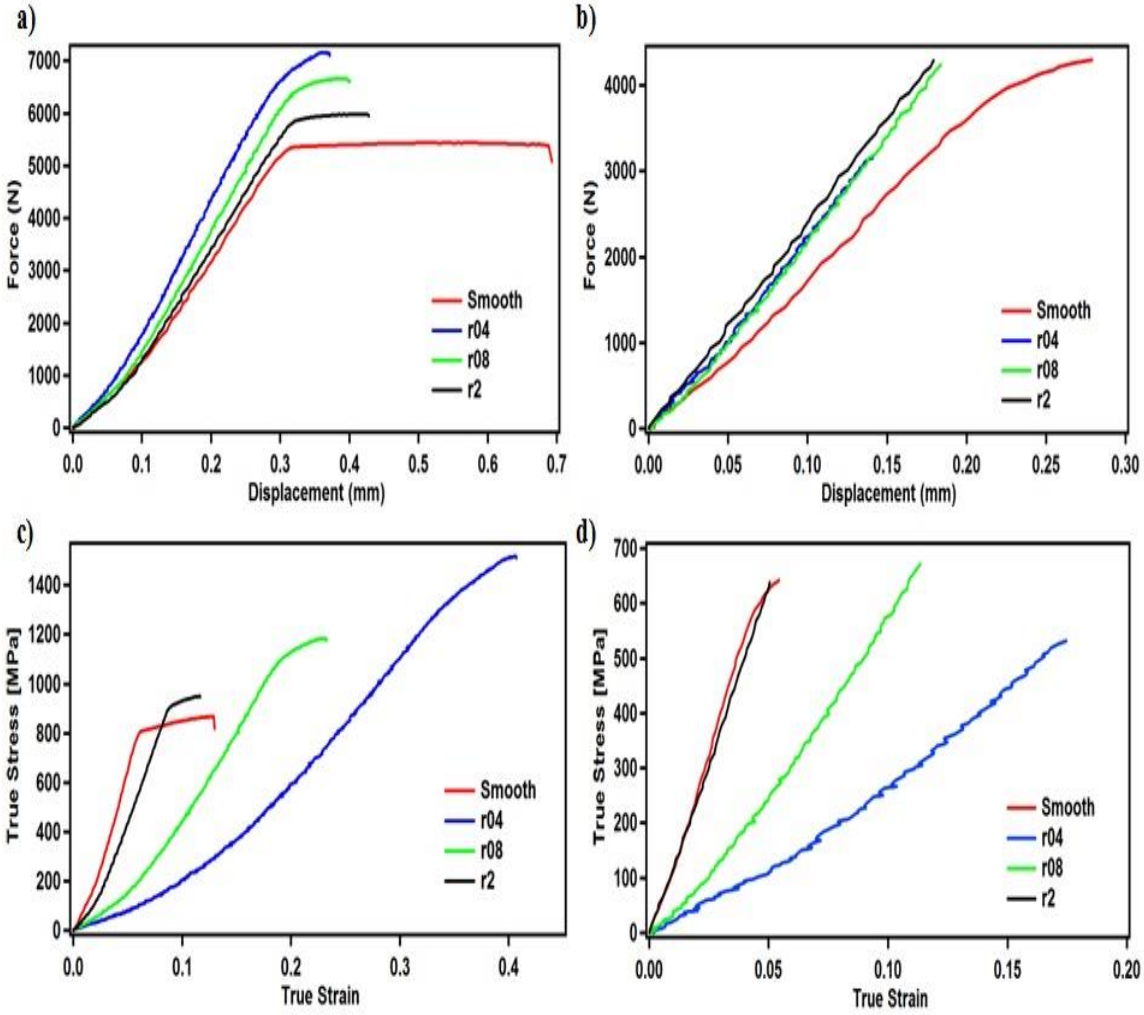

Figure 4.5.1 Force versus displacement graphs of Al 7068 alloy a) along the rolling direction b) perpendicular to the rolling direction and true stress – true strain behavior of Al 7068 alloy c) along the rolling direction d) perpendicular to the rolling direction

Rolling Direction	Notch Radius (mm)	Yield Strength (MPa)	Tensile Strength (MPa)	Engineering Strain at fracture (mm/mm)	True Strain at fracture (mm/mm)
Along The Rolling Direction	Smooth (0)	708	819	0.10021	0.0955
	0.4	837	1510	0.49323	0.40094

	0.8	812	1170	0.25052	0.22356
	2	763	947	0.11855	0.11204
Perpendicular to The Rolling Direction	Smooth (0)	503	642	0.05579	0.05429
	0.4	-	531	0.19076	0.17459
	0.8	-	671	0.12018	0.11349
	2	-	638	0.05179	0.05049

Table 4.5.1 Yield strength, tensile strength and elongation values of smooth and notch specimens

Figure4.5.2 shows the effect of the rolling direction on the mechanical response of Al 7068 alloy. It is obvious that the mechanical properties of the Al 7068 alloy are dramatically deteriorated when the rolling direction of the specimen is changed from along the rolling direction to perpendicular to the rolling direction. In particular, when the direction is changed, mechanical strength and ductility values drop by at least 21.6 % and 44.3 %, respectively. On the contrary, within the elastic range, Al 7068 alloy perpendicular to the rolling direction has greater strength values at the same strain compared to materials along the rolling direction. However, they are brittle and sudden failure occurs before yield point. Therefore, Al 7068 alloy in the direction perpendicular to the rolling direction can be safely used over Al 7068 alloy along the rolling direction for applications that do not require high stress values. The current finding proves that Al 7068 material has anisotropic properties and the determination of these is very crucial for engineering design of this material.

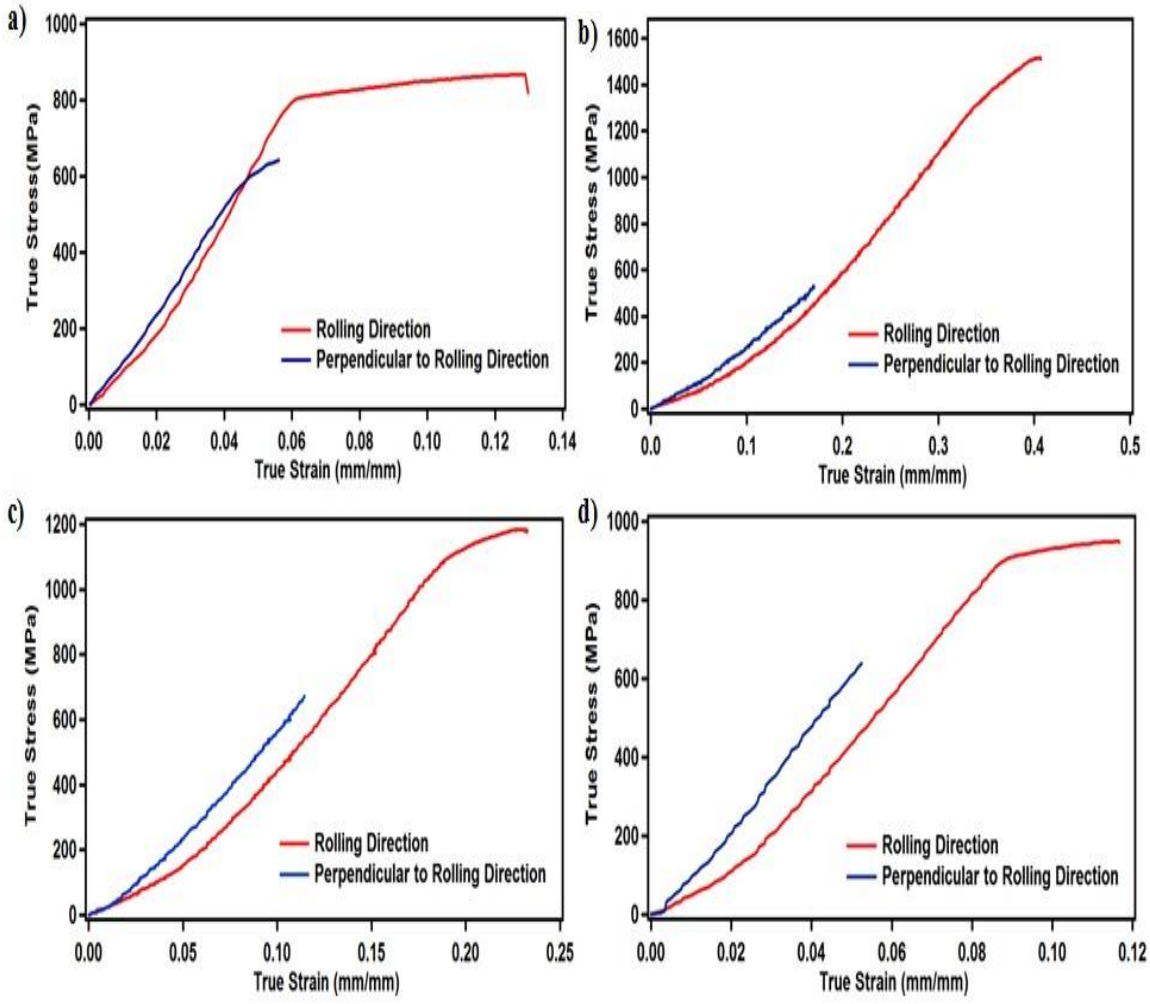

Figure 4.5.2 Comparison of the tensile behavior between the rolling direction and perpendicular to the rolling direction a) smooth specimens b) R0.4 c) R0.8 d) R2

The relationship between STF and equivalent failure strain for specimen along and perpendicular to the rolling direction are given in Figure 4.5.3 and Figure 4.5.4, respectively. STF and equivalent plastic strain at fracture values were calculated by using equations 4.4.5 and 4.4.6, respectively. For all specimens in both directions, the equivalent plastic strain at fracture is generally inversely proportional to STF. This behavior is expected since it is well know that as the STF increases, the structural degradation occurs earlier under tensile loading and corresponds well with previous studies [53, 54]. Yet, this behavior depends on the material and the rolling direction as shown in Figure 4.5.4. The change in STF from 0.33 to 0.65 caused a slight increase on the equivalent plastic strain at fracture for the material perpendicular to the rolling direction. This behavior shows that a critical notch radius might enhance the failure strain of the Al 7068 alloy perpendicular to the rolling direction.

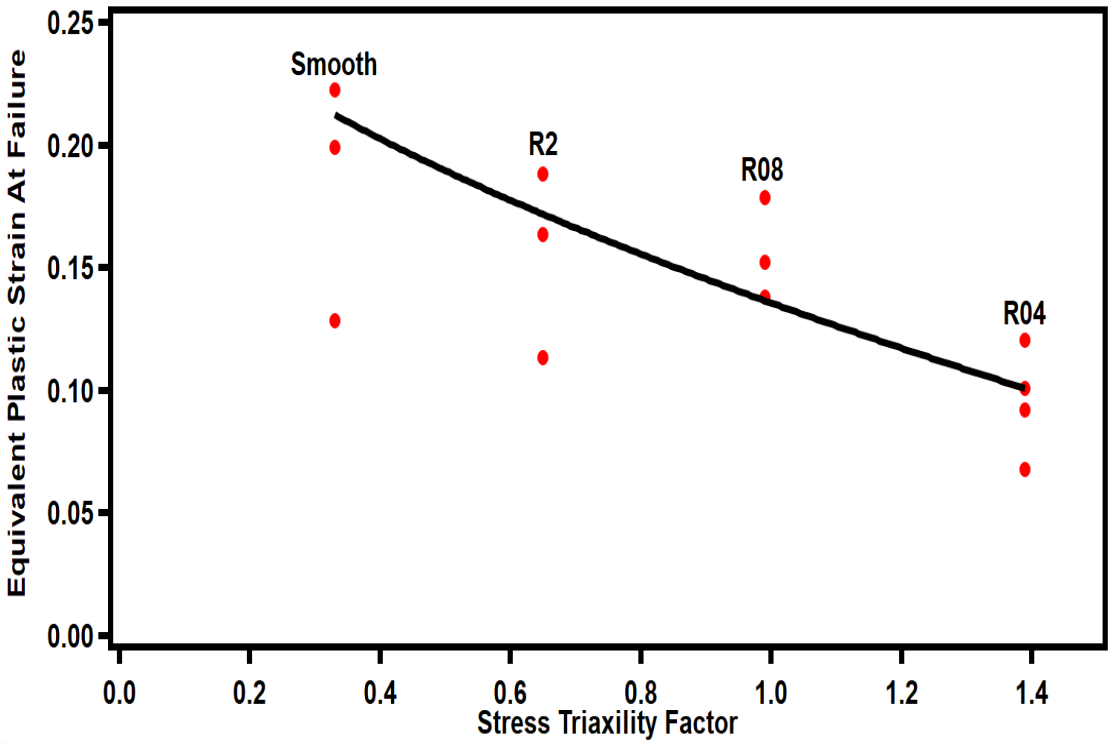

Figure 4.5.3 Equivalent plastic strain to fracture vs. STF for the specimen in the rolling direction

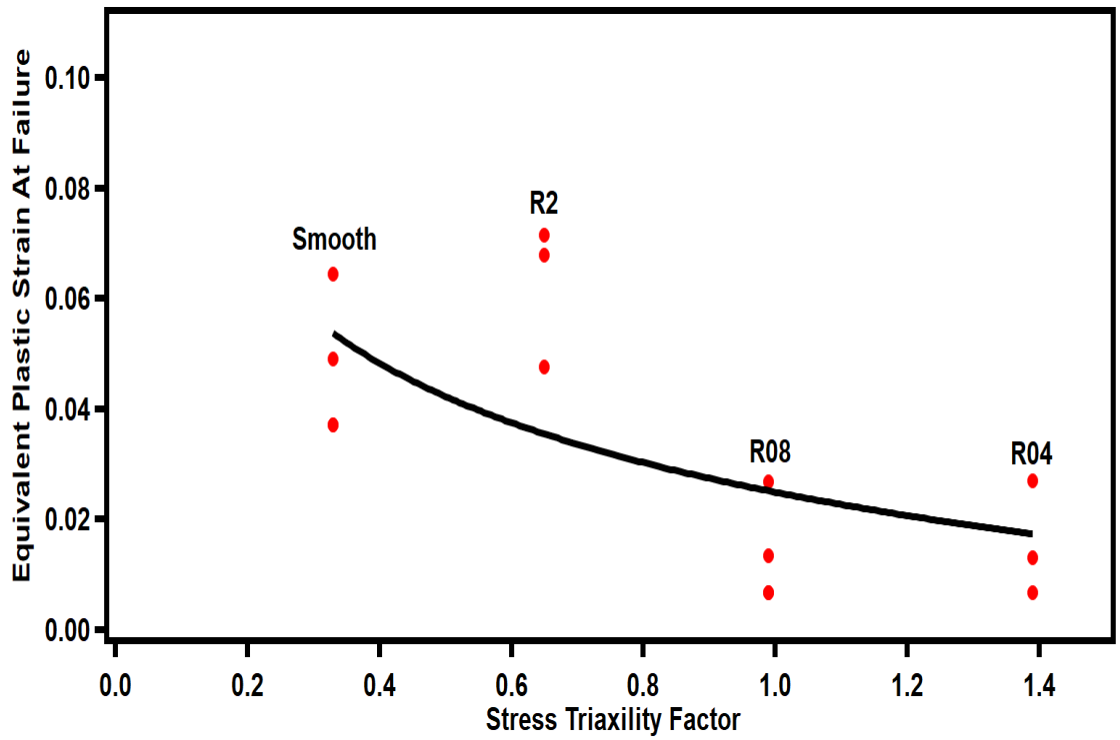

Figure 4.5.4 Equivalent plastic strain to fracture vs. STF for the specimen perpendicular to the rolling direction

J-C damage model constants, D_1, D_2 and D_3 of the Al 7068-T651 alloy were computed by equation 4.4.7 using Levenberg-Marquardt optimization method. Specifically, a Matlab script was prepared to solve the overdetermined system. By using maximum, average and minimum values of the equivalent plastic strain at fracture, which are shown as red dots in Figure 4.5.3 and Figure 4.5.4, three different J-C damage constants for different application areas were computed. The computed J-C damage parameters are listed in Table 4.5.2, Table 4.5.3 and Table 4.5.4. In the current literature, the J-C damage constant for different materials are generally calculated based on average failure strain and given as an average J-C damage parameters [55]. However, the average J-C damage parameters should be used to simulate the mechanical responses of different applications, where the reliability is not the main concern. For instance, for a car design, average J-C damage parameters (Table 4.5.3) can be used in FE simulations since both cost and safety are significant for automobile industry.

In this article, in addition to J-C damage parameters, which were calculated based on average equivalent strain values, J-C damage model constants based on maximum and minimum equivalent strain values were also determined since these can be used for the simulation of different application areas. Table 4.5.2 lists the J-C damage model constants for Al 7068 alloy based on maximum equivalent plastic strain values. When safety is not the main concern for a design, these J-C damage constants (in Table 4.5.2) can be used in FE simulations, such as demanding applications. For instance, the maintenance period for race cars is very frequent and the main concern on the design of race cars is to manufacture the most lightweight and compact race car so the J-C damage parameters listed in the Table 4.5.2 can be used for the FE simulations of these kinds of application areas. On the other hand, if the material will be used applications where safety is the primary concern, such as elevators, the J-C damage model constants based on minimum equivalent plastic strain values (Table 4.5.4) can be utilized. Thus, this article opens a new venue for the usage of Al 7068 alloy for different application areas. Consequently, this study is one of the first studies, which precisely determine the J-C damage parameters of Al 7068 alloy both along the rolling direction and perpendicular to the rolling direction for different application areas.

J-C Damage Constant	Rolling Direction	Perpendicular to the rolling direction
D1	0.1211	0.0269
D2	0.4535	0.0374
D3	-2.6445	-4.1040

Table 4.5.2 Johnson-Cook damage model constants for Al 7068-T651 alloy with maximum equivalent plastic strain values

J-C Damage Constant	Rolling Direction	Perpendicular to the rolling direction
D1	0.1009	0.0130
D2	0.1214	0.0359
D3	-0.9150	-3.1844

Table 4.5.3 Johnson-Cook damage model constants for Al 7068-T651 alloy with average equivalent plastic strain values

J-C Damage Constant	Rolling Direction	Perpendicular to the rolling direction
D1	0.0678	0.0066
D2	0.0604	0.0304
D3	-0.0251	-3.1844

Table 4.5.4 Johnson-Cook damage model constants for Al 7068-T651 alloy with average equivalent plastic strain values

Chapter 5

5 Conclusions

In this study, the effects of the rolling direction and STF on the mechanical response of Al 7068 alloy were investigated. The results are very accurate since each experiment was repeated seven times. Then, by utilizing the Levenberg-Marquardt optimization method, which was applied on an iterative code through Matlab, J-C damage model constants, based on maximum and minimum equivalent strain values were also determined since these can be used for the simulation of different applications.

With this study, it can be concluded that as the STF is increasing, both strength and ductility of the alloy also increase for the specimen along the rolling direction while the smooth specimen has the greatest strength at the same elastic strain values compared to other specimens. On the contrary, for specimens in perpendicular to rolling direction, as the STF increases, only ductility of the alloy increases. It was also concluded that Al 7068-T651 alloy has anisotropic mechanical properties and changing the direction from along the rolling to perpendicular to the rolling direction deteriorates the mechanical properties of the Al7068-T651 alloy. On the contrary, within the elastic range, Al 7068 alloy perpendicular to the rolling direction has greater strength values at the same strain compared to materials along the rolling direction. Thus, specimen perpendicular to the rolling direction can be used over Al 7068 alloy along rolling direction in applications where high ductility is not required. Furthermore, even though as the stress triaxiality increases, the failure strain of the Al 7068 along the rolling direction always decreases, it was observed that a critical notch radius might enhance the failure strain of the Al 7068 alloy perpendicular to the rolling direction.

Overall, this study investigates for the first time the effects of rolling direction and STF on the mechanical response of Al 7068 alloy accurately and corresponding J-C damage parameters were determined for different application areas.

Chapter 6

6 Final Remarks and Future Work

Al 7068 alloys have been investigated in this work because of its promising mechanical properties, such as density, good ductility and high strength. They are mainly used in aerospace and military applications. In this study, tensile tests of Al 7068 T651 alloy were conducted to obtain J-C damage parameters of D_1, D_2 and D_3. By using Levenberg-Marquardt optimization method, these parameters were computed for different application areas by considering maximum, average and minimum equivalent plastic strain values. For instance; when safety the is main concern for a design, J-C damage model constants based on minimum equivalent plastic strain values can be used in FE simulations. However, if the design is not too conservative and is for demanding applications, J-C damage model constants based on maximum equivalent plastic strain values can be used in FE simulations

In this study, firstly, the effects of Stress Triaxiality Factor (STF) and rolling direction on the mechanical response of Al 7068 were investigated. It is observed that the mechanical properties like mechanical strength and ductility of the Al 7068 alloy are dramatically deteriorated when the rolling direction of the specimen is changed from along the rolling direction to perpendicular to the rolling direction. The findings of this study proves that Al 7068 material has anisotropic properties and the determination of mechanical properties of Al 7068 along different rolling direction and under different STF is very important for engineering design of this material. In addition, J-C damage parameters, D_1, D_2 and D_3, of Al 7068 along different rolling directions are also determined.

Future works of this study will be the calculation of other damage parameters, D_4 and D_5. To calculate D_4, we will conduct Split Hopkinson pressure bar tests at different

strain rates. In addition, to calculate D_5, we will conduct Split Hopkinson pressure bar tests at different temperatures. To sum up, all the J-C damage model constants will be calculated for Al 7068 T651 alloys along both rolling direction and this will open a new venue for the usage of this alloy in different application areas.

Also, the fractured specimens' SEM images will be investigated to understand the microstructure and failure mode. In addition, the effects of notch radius and rolling direction on the microstructure of this alloy will be observed.

BIBLIOGRAPHY

1. Gourier-Fréry, C. & Fréry, N. Aluminium. *EMC - Toxicologie-Pathologie***1,** 79–95 (2004).
2. Davis, J. R. Aluminum and Aluminum Alloys. *Light Met. Alloy.* 66 (2001). doi:10.1361/autb2001p351
3. Cole, G. S. & Sherman, A. M. Light weight materials for automotive applications. *Mater. Charact.***35,** 3–9 (1995).
4. Zhang, D. N., Shangguan, Q. Q., Xie, C. J. & Liu, F. A modified Johnson-Cook model of dynamic tensile behaviors for 7075-T6 aluminum alloy. *J. Alloys Compd.***619,** 186–194 (2015).
5. Dursun, T. & Soutis, C. Recent developments in advanced aircraft aluminium alloys. *Materials and Design***56,** 862–871 (2014).
6. Hecker, S. S. Formability of Aluminum Alloy Sheets. *J. Eng. Mater. Technol.***97,** 66 (1975).
7. Anon. ALUMINUM VS STEEL FOR BODY PANELS. *Automot. Eng. Int.***84,** (1976).
8. Donaldson, D. & Raahauge, B. E. *Essential Readings in Light Metals: Alumina and Bauxite, Volume 1*. *Essential Readings in Light Metals: Alumina and Bauxite, Volume 1***1,** (2013).
9. Tabereaux, A. T. & Peterson, R. D. in *Treatise on Process Metallurgy***3,** 839–917 (2014).
10. Hond, R. Den, Hiralal, I. & Rijkeboer, A. in *Essential Readings in Light Metals: Alumina and Bauxite, Volume 1***1,** 528–533 (2013).
11. Anon. ALUMINUM. *Eng. Min. J.***184,** (1983).
12. Polmear, I. J. 2 - Physical metallurgy of aluminium alloys. *Light Alloy. (Fourth Ed.* 29–96 (2005). doi:http://dx.doi.org/10.1016/B978-075066371-7/50006-2
13. Kaufman, J. G. & International, a S. M. *Introduction to Aluminum Alloys and Tempers*. *ASM International* (2000).
14. The Aluminum Association Inc. International Alloy Designations and Chemical Composition Limits for Wrought Aluminum and Wrought Aluminum Alloys. *Alum. Assoc. Arlington, Virginia* 28 (2006).

15. Davis, J. R. *ASM Specialty Handbook: Aluminum and Aluminum Alloys*. *ASM International* (1993).
16. Zolotorevsky, V. S., Belov, N. A. & Glazoff, M. V. *Casting Aluminum Alloys*. *Casting Aluminum Alloys* (2007). doi:10.1016/B978-0-08-045370-5.X5001-9
17. Cobden, R. & Banbury, A. Aluminium: Physical Properties, Characteristics and Alloys. *Talal***1994,** 60 (1994).
18. Aalco Metals Ltd. *Aluminum Alloy Temper Designations*. (2017).
19. Wei, R. P., Gao, M. & Pao, P. S. The role of magnesium in CF and SCC of 7000 series aluminum alloys. *Scr. Metall.***18,** 1195–1198 (1984).
20. Smiths Metal Centers. *7068 Aluminum Alloy Technical Datasheet*. (2017).
21. Minnicino, M., Gray, D. & Moy, P. *Aluminum Alloy 7068 Mechanical Characterization*. (2009).
22. Kaiser Aluminium. *Al 7068 alloy*. (2008).
23. SAE International. *Aluminum 7068-T6 ; 7068-T6511 Rod & Bar, Metals and Alloys in the Unified Numbering System*. *Society of Automotive Engineers, Inc. and American Society for Testing and Materials 8TH ED.* (1999).
24. Hutton, D. V. Fundamentals of Finite Element Analysis. *Textbook (Important)* 494 (2004). doi:10.1017/CBO9781107415324.004
25. Fish, J. & Belytschko, T. *A First Course in Finite Elements*. *A First Course in Finite Elements* (2007). doi:10.1002/9780470510858
26. Larson, M. G. & Bengzon, F. *The Finite ElementMethod: Theory, Implementation, and Applications*. *Fea* (2010). doi:10.1007/978-3-642-02475-7
27. Poulachon, G., Moisan, A. & Jawahir, I. S. On modelling the influence of thermo-mechanical behavior in chip formation during hard turning of 100Cr6 bearing steel. *CIRP Ann. - Manuf. Technol.* (2001). doi:10.1016/S0007-8506(07)62064-2
28. Altan, T., Al-Zkeri, İ. & Sartkulvanich, P. Process Modelling of High Speed Cutting Using 2D FEM. (2015).
29. Zhang, Y., Outeiro, J. C. & Mabrouki, T. On the selection of Johnson-Cook constitutive model parameters for Ti-6Al-4V using three types of numerical models of orthogonal cutting. in *Procedia CIRP* (2015). doi:10.1016/j.procir.2015.03.052
30. Meyer, H. W. A Modified Zerilli-Armstrong Constitutive Model Describing the Strength and Localizing Behavior of Ti-6Al-4V. *Mater. Res.* (2006).

doi:C5693BE1CB5A3F7FACD0ABB446321E1A

31. Jivishov, V. & Rzayev, E. Influence of Material Models Used in Finite Element Modeling on Cutting Forces in Machining. *IOP Conf. Ser. Mater. Sci. Eng.***142,** (2016).
32. Umbrello, D., Hua, J. & Shivpuri, R. Hardness-based flow stress and fracture models for numerical simulation of hard machining AISI 52100 bearing steel. *Mater. Sci. Eng. A* (2004). doi:10.1016/j.msea.2004.01.012
33. Sheppard, T. & Wright, D. S. Determination of flow stress: Part 1 constitutive equation for aluminium alloys at elevated temperatures. *Met. Technol.* (1979). doi:10.1179/030716979803276264
34. Johnson, G. R. & Cook, W. H. Fracture characteristics of three metals subjected to various strains, strain rates, temperatures and pressures. *Eng. Fract. Mech.* (1985). doi:10.1016/0013-7944(85)90052-9
35. Manes, A., Peroni, L., Scapin, M. & Giglio, M. Analysis of strain rate behavior of an Al 6061 T6 alloy. in *Procedia Engineering* (2011). doi:10.1016/j.proeng.2011.04.573
36. Brar, N. S. & Joshi, V. S. Anisotropic effects on constitutive model parameters of aluminum alloys. *AIP Conf. Proc.***1426,** 72–75 (2012).
37. Tan, J. Q. *et al.* A modified Johnson-Cook model for tensile flow behaviors of 7050-T7451 aluminum alloy at high strain rates. *Mater. Sci. Eng. A***631,** 214–219 (2015).
38. Bobbili, R., Paman, A. & Madhu, V. High strain rate tensile behavior of Al-4.8Cu-1.2Mg alloy. *Mater. Sci. Eng. A***651,** 753–762 (2016).
39. Courant, R. Variational methods for the solution of problems of equilibrium and vibrations. *Bull. Am. Math. Soc.***49,** 1–24 (1943).
40. Zienkiewicz, O. C., Taylor, R. L. & Zhu, J. Z. The Finite Element Method: Its Basis and Fundamentals, Sixth edition. *Int. J. Numer. Methods Eng.* 733 (2005). doi:10.1016/B978-1-85617-633-0.00015-0
41. HINTON, E. & IRONS, B. LEAST SQUARES SMOOTHING OF EXPERIMENTAL DATA USING FINITE ELEMENTS. *Strain***4,** 24–27 (1968).
42. Strang, G. & Fix, G. J. *An analysis of the finite element method*. *An Analysis of the Finite Element Method***212,** (1973).
43. Valoppi, B., Bruschi, S., Ghiotti, A. & Shivpuri, R. Johnson-Cook based criterion incorporating stress triaxiality and deviatoric effect for predicting elevated

temperature ductility of titanium alloy sheets. *Int. J. Mech. Sci.***123,** 94–105 (2017).

44. Liu, R. *et al.* An enhanced constitutive material model for machining of Ti-6Al-4V alloy. *J. Mater. Process. Technol.***213,** 2238–2246 (2013).
45. Chen, G., Ren, C., Qin, X. & Li, J. Temperature dependent work hardening in Ti–6Al–4V alloy over large temperature and strain rate ranges: Experiments and constitutive modeling. *Mater. Des.***83,** 598–610 (2015).
46. Thepsonthi, T. & Özel, T. 3-D finite element process simulation of micro-end milling Ti-6Al-4V titanium alloy: Experimental validations on chip flow and tool wear. *J. Mater. Process. Technol.***221,** 128–145 (2015).
47. Onal, O., Bal, B., Canadinc, D. & Akdari, E. Experimental and Numerical Evaluation of Thickness Reduction in Steel Plate Heat Exchangers. *J. Eng. Mater. Technol. Trans. ASME***137,** (2015).
48. Onal, O. *et al.* Microstructure-based modeling of the impact response of a biomedical niobium–zirconium alloy. *J. Mater. Res.***29,** 1123–1134 (2014).
49. Vening Meinesz, F. A. Elasticity and plasticity. *Appl. Sci. Res. Sect. A***6,** 205–225 (1956).
50. Algarni, M., Bai, Y. & Choi, Y. A study of Inconel 718 dependency on stress triaxiality and Lode angle in plastic deformation and ductile fracture. *Eng. Fract. Mech.***147,** 140–157 (2015).
51. Keshavarz, A., Ghajar, R. & Mirone, G. A new experimental failure model based on triaxiality factor and Lode angle for X-100 pipeline steel. *Int. J. Mech. Sci.***80,** 175–182 (2014).
52. Senthil, K., Iqbal, M. A., Chandel, P. S. & Gupta, N. . Study of the constitutive behavior of 7075-T651 aluminum alloy. *Int. J. Impact Eng.***000,** (2017).
53. Brar, N. S., Joshi, V. S. & Harris, B. W. Constitutive model constants for Al7075-T651 and Al7075-T6. *AIP Conf. Proc.***1195,** 945–948 (2009).
54. Mirzajanzadeh, M. & Canadinc, D. A microstructure-sensitive model for simulating the impact response of an high-manganese austenitic steel. *J. Eng. Mater. Technol.***138,** 1–14 (2016).
55. Majzoobi, G. H. & Dehgolan, F. R. Determination of the constants of damage models. *Procedia Eng.***10,** 764–773 (2011).